2018년 8월

박사학위논문

Extra Sensitive Silicon Quantum Dots-embedded Porous Silicon Nanoparticles

조선대학교 대학원

탄소소재학과

김 진 수

Extra Sensitive Silicon Quantum Dots-embedded Porous Silicon Nanoparticles

초고감도 실리콘 양자점이 부착된 다공성 실리콘 나노입자 연구

2018년 8월 24일

조선대학교 대학원

탄소소재학과

김 진 수

Extra Sensitive Silicon Quantum Dots-embedded Porous Silicon Nanoparticles

지도교수 손 홍 래

이 논문을 이학박사학위 신청 논문으로 제출함
2018년 04월

조선대학교 대학원

탄소소재학과

김 진 수

김진수의 박사학위논문을 인준함

위원장 조선대학교 교수 임 종 국 (인)

위 원 조선대학교 교수 손 홍 래 (인)

위 원 조선대학교 교수 이 재 관 (인)

위 원 조선대학교 교수 김 호 중 (인)

위 원 세한대학교 교수 고 영 춘 (인)

2018년 06월

조선대학교 대학원

TABLE OF CONTENTS

LIST OF SYMBOLS AND ABBREVIATIONS

Å	Angstrom
β	Beta
cm	Centimeter
℃	Celsius temperature scale
$\mathbf{m^3}$	Cubic Meter
d	Diameter
δ	Delta
ε	Epsilon
λ_{em}	Emission Wavelength
fg	Femtogram
d	Film thickness
g	Gram
$\mathbf{h^+}$	Hole
h	Hour
kJ	Kilojoule
λ	lambda
L	Liter
m	Mass
M	Molarity
㎛	Micrometer
mg	Milligram
mA	Milliampere
mmol	Millimole
mL	Milliliter
λ_{max}	Maximum Wavelength
μ	Mu
***μ*M**	Micromolarity
$\mathbf{M_w}$	Molecular Weight
㎍	Microgram

MHz	MegaHertz
ν	Nu
nm	Nanometer
Ω	Ohm
π	Pi
%	Percent
n	Refractive Index
σ	Sigma
T	Thickness
t	Time
vs	Versus
V	Volume
W	Watt
A.U.	Arbitrary Units
Al	Aluminium
AIE	Aggregation-Induced Emission
BET	Brunauer-Emmett-Teller
BuLi	Butyllithium
Cu	Copper
CWA	Chemical Warfare Agents
c-Si	Crystalline Silicon
CCD	Charge-Coupled Detector
CdSe	Cadmium Selenide
DCP	Diethyl Chlorophosphate
DFP	Diisopropyl Phosphonate
DEEP	Diethyl Ethylphosphonate
DMMP	Dimethyl Methylphosphonate
DNA	Deoxyribonucleic Acid
DMF	Dimethyl Formaldehyde
DNT	Dinitrotoluene
EL	Electroluminescence
EDS	Energy Dispersive X-ray Spectrometry

FIPOS	Full Isolated Porous Oxidized Silicon
FWHM	Full-Width at Half-Maximum
F-P	Fabry-Pérot
FT-IR	Fourier Transform Infrared Spectroscopy
HOMO	Highest Ocuppied Molecular Orbital
HF	Hydrofluoric Acid
IC	Integrated Circuit
InP	Indium phosphate
InAs	Indium Arsenide
LCT	Lethal Concentration
LED	Light Emitting Diode
LUMO	Lowest Unoccupied Molecular Orbital
$LiAlH_4$	Lithium Aluminum Hydride
MEMS	Micro Electro Mechanical Systems
MALDI	Matrix-Assisted Laser Desorption Ionization
Mg_2Si	Magnesium Silicide
NaOH	Sodium Hydroxide
NA	Nerve Agents
NA	Nanoaggregates
NP	Nanoparticle
NMR	Nuclear Magnetic Resonance
OSHA	Occupational Safety and Health Administration
PSi	Porous Silicon
Pt	Platinum
PL	Photoluminescence
PA	Picric Acid
PBS	Phosphate Buffer Solution
PSA	Particle Size Analyzer
ppm	Part Per Million
ppb	Part Per Billion
ppt	Part Per Trillion
pmol	Picomole
R.T.	Room Temperature
SAED	Selected Area Electron Diffraction
Si	Silicon
SiO_2	Silicon Dioxide
sec	Second

SAW	Surface Acoustic Wave
SOI	Silicon-On-Insulator
S-V Eqn	Stern-Volmer Equation
SWNT	Single-walled Nanotube
TLC	Thin-Layer Chromatography
TNT	Trinitrotoluene
TMS	Tetramethylsilane
THF	Tetrahydrofuran
TMEDA	Tetramethyl Ethylene Diamine
TEP	Triethylphosphate
TEOS	Tetraethyl orthosilicate
TOPO	Tri-*n*-octylphosphineoxide
UV	Ultraviolet
UV-Vis	Ultraviolet-Visible

LIST OF TABLES

LIST OF FIGURES

PART I. QUANTUM DOTS FOR EXPLOSIVE SENSORS

Part II. EXPLOSIVE SENSOR PLATFORM BASED ON SILICON QUANTUM DOTS-EMBEDDED POROUS SILICON

초 록

광결정 다공성실리콘과 실리콘 양자점을 기초로한 나노센서 연구

박사과정 : 김 진 수
지도교수 : 손 홍 래
조선대학교 탄소소재학과

최근 수 십 년간 전기·전자 및 금속·반도체기술이 눈부신 발전을 이룩하였다면 21세기 현대과학에서는 새로운 형태나 특성을 연구하는 영역으로 나노과학 및 나노기술이 급속히 발전하고 있다. 현대 화학이 여러 분야로 세분화되고, 전문화되어지면서 광화학 이나 나노화학 에 대한 관심도가 매우 높아지고 있다. 특히, 나노소재를 이용한 분야가 매우 빠른 속도로 발전하고 있다. 나노과학은 나노소재의 합성 및 응용분야로 분류된다. “나노센서” 는 나노과학의 한 응용분야로서 분자 수준의 조작이 가능한 분자센서의 집적화 또는 나노소재 나 나노구조물 의 특성을 이용한 센서를 의미한다. 나노소재로는 나노다공질재료 , 금속 및 반도체소재의 나노와이어, 나노입자, 나노튜브 등이 있으며 기질을 인지 또는 감지할 수 있는 나노소재로부터 장치를 만들었을 경우 나노센서라 일컫는다.

최근 나노센서 또는 나노바이오센서 등에 대한 관심이 나노과학의 한 분야로서 지대한 관심의 대상이 되고 있는데 그 이유는 고감도, 초소형의 센서 구현을 통해서 생명현상인 분자 간의 상호작용을 나노크기의 수준에서 탐구하려는 학문적인 관심과 함께 응용적인 측면에서 보건의

료, 식품, 환경, 국방 등의 다양한 분야에서 활용되는 센서를 개발하기 위한 실질적인 중요성 때문에 학계와 연구소, 그리고 산업체에서 활발히 연구되고 있다. 특히 나노 신소재 개발 분야는 기초과학에서부터 첨단과학까지의 융합학제 간 학문 분야로 미래기술의 선점 및 국가경쟁력 확보에 있어서 우위를 차지하는데 중요한 역할을 할 것으로 기대된다.

본 연구는 현재 전 세계 폭발물로 인한 테러위협이 증가함에 따른 효과적인 폭발물 스크리닝 시스템에 대한 요구에 응한 것이다. 지금 ion mobility spectrometry (IMS) 및 가스 크로마토그래피와 같은 현재의 폭발물 감지 기술에 사용되는 대부분의 일반적인 탐지 기술은 위에 요구를 충족시키기에는 제한적인 부분인 많다. 사용하기 위해 많은 시간과 넓은 공간이 필요로 때문이다. 이 연구의 초점은 위의 문제에 대해 가능한 해결책의 하나로서, 다공성 실리콘을 사용한 감지 플랫폼의 연구 및 계발이다. 다공성 실리콘의 기공 크기를 자유롭게 조율 가능하며, 효율적인 가시광선 방출과 큰 비표면적과 같은 흥미로운 특징을 통해 폭발물 감지기를 제조하는 데 활용할 수 있다. 또한 비교적 간단한 감지기 구조의 구현을 가능하게 한다.

Part I.

QUANTUM DOTS FOR EXPLOSIVE SENSORS

Chapter One

Detection of PETN and RDX Based on CdSe Quantum Dots

1.1 Introduction

The threats of explosives-based terrorism has been ever increasing. Thus, techniques detecting the concealed bombs are of urgent importance. Unfortunately the current screening systems are too slow, too big, and very expensive to cope with this terrorism. This calls for a small and easy to use device that can be massively deployed where needed.[1] Chemo-sensor might be one of alternatives, [2], [3] which possesses a relatively simple detection method with a low-cost and easy-fit into a small handheld device. CdSe quantum dots (QDs) well-characterized by Bawendi et al.[4] are a new class of fluorescent nanoprobes for sensing and imaging applications. Attention has been drawn to detection of nitro-aromatics such as trinitrotoluene (TNT, vapor pressure = 7 ppb at 25 ℃) for last decades. However, it is also very important to detect other types of explosives, such as nitro-amines (trinitroperhydrotriazine, RDX) and nitrate ester (pentaerythritol tetranitrate, PETN). Because they have a high lying lowest unoccupied molecular orbital (LUMO) compared to TNT and the vapor pressures of PETN and RDX are extremely low such as 18 and 6 ppt at 25 ℃, respectively.[5] To date, only fewpublications have been reported, for example, CdSe/ZnS core/shell QDs

[6] and surface-modified CdTe QDs [7] for TNT detections. In this study, we report successful detection of PETN and RDX based on CdSe QDs for the first time.

1.2 Results and Discussion

CdSe QDs were synthesized according to the literature by Peng et al. [8] and characterized in Figure 1.1 Emission maximum wavelength of photoluminescence (PL) was 520 nm in PL spectrum and absorption wavelength was 410 nm in UV/Vis. spectrum. CdSe QDs were utilized for sensing experiment of PETN and RDX through observing quenching of PL emission caused by electron transfer from electron-rich species of CdSe QDs to electron-deficient molecules of nitroamine or nitrate ester. As shown in Figure 1.2, the PL of CdSe QDs quenched rather linearly according to the amount of PETN (a) and RDX (b) was introduced. The quenching by electron transfer as a sensing mechanism showed different results for PETN and RDX, more amount of RDX had to be added in order to observe similar quenching effect.

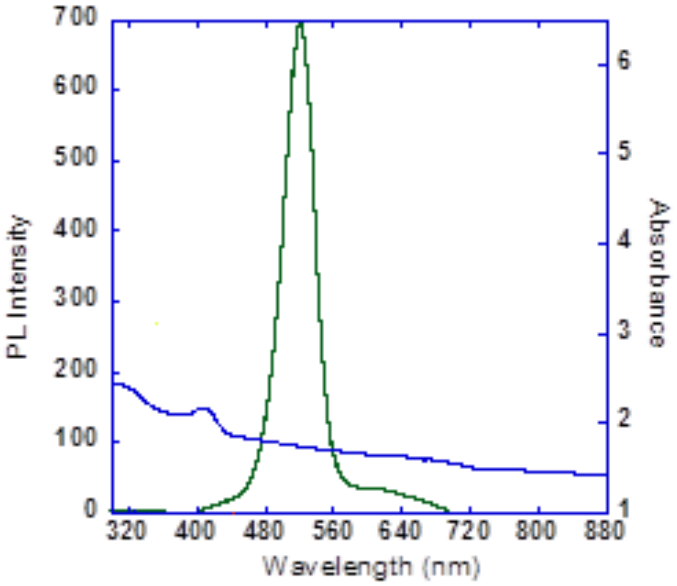

Figure. 1.1 UV absorption and PL spectra of CdSe QDs

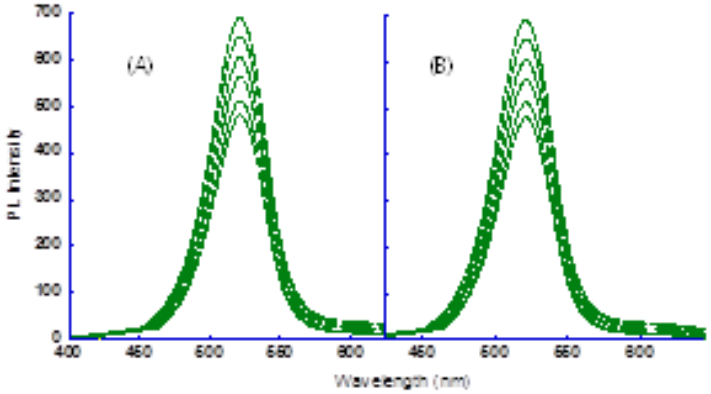

Figure. 1.2 PL quenching spectra of CdSe QDs recorded from top every addition of 0 M, 9.213 × 10^{-7} M, 1.79 × 10^{-6} M, 3.389 × 10^{-6} M, 4.125 × 10^{-6} M, and 4.825 × 10^{-6} M of PETN (A) and 0 M, 2.143 × 10^{-6} M, 4.092 × 10^{-6} M, 5.3872 × 10^{-6} M, 7.503 × 10^{-6} M, and 9.004 × 10^{-6} M of RDX (B) in octadeylamine.

Stern.Volmer constants were measured to analyze the PL-quenching efficiency of the analytes for the CdSe QDs. Stern.Volmer relationship is particularly useful tool for analyzing PL-quenching efficiencies for comparison. Stern-Volmer constant (K_{sv}) is described by the equation:

$$\frac{I_f^o}{I_f} = 1 + K_{sv} \cdot [Q] \qquad (1)$$

where I0 f is the intensity without a quencher, If is the intensity with a quencher, [Q] is the concentration of the quencher, K_{sv} is the quencher rate coefficient, and τ 0 is the lifetime of emission in exited state. A linear Stern-Volmer relationship was obtained in both cases. As seen in Figure 1.3, PL-quenching efficiency for PETN is higher than that of RDX, which is because of the low-lying LUMO energy level of PETN. Highest occupied molecular orbital (HOMO) and LUMO energy levels of PETN, RDX, and 2,3-dimethyl-2,3-dinitrobutane (DMNB) were reported by using Gaussian 03 Suite of programs at the B3LYP/6.31G* level in the literature[9] and summarized in Table 1. According to K_{sv} from Table 1, quenching efficiency of PETN is 140% higher than that of RDX due to the low-lying LUMO. Previously reported Stern-Volmer constants indicating quenching efficiencies for RDX based on dye-modified silica nanoparticles[10] and amine-capped ZnS:Mn QDs[11] were 2011 and 1530, respectively. Therefore, our results indicate that detection efficiency of CdSe QDs for RDX is 27 to 35 times higher that of previously reported sensing materials.

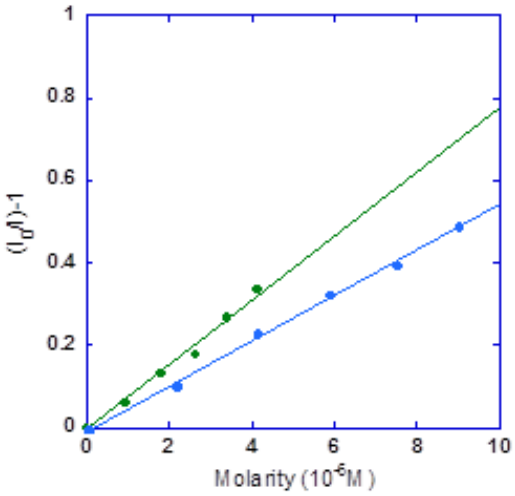

Figure. 1.3 The Stern-Volmer plots for quenching efficiency for PETN (green) and RDX (blue)

Table. 1.1 HOMO and LUMO energies levels calculated for PETN, RDX, and DMNB and K_{sv}

Analytes	LUMO (eV)	HOMO (eV)	K_{sv} (M^{-1})
PETN	-3.075	-8.707	77,988
RDX	-2.531	-8.245	54,875
DMNB	-2.068	-8.027	0

DMNB is a nitroalkyl compound and explosive taggant with high vapor pressure that explosive manufacturers are required add during the production, so that canines can sense it with their nose easily. However, DMNB possesses the highest LUMO energy level among those mentioned three analytes, thus it would be inconvenient to detect by electron transfer mechanism. Therefore, we conducted experiment with DMNB which might be very challengeable. As seen in Figure 1.4, PL of CdSe QDs did not quench at all which is because of the highest lying LUMO of DMNB. The conduction band edge of CdSe QDs probably had lower LUMO energy level than that of DMNB, making it difficult for electrons to transfer.

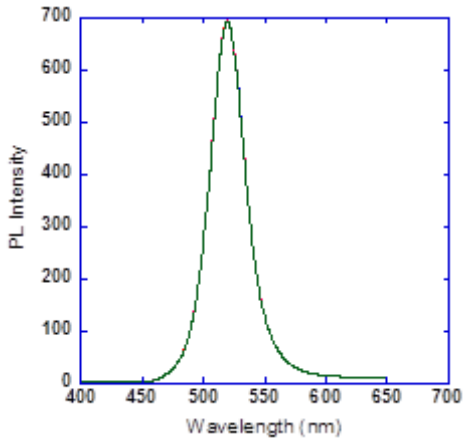

Figure. 1.4 PL of CdSe QDs did not quench at all which is due to the highest lying LUMO of DMNB

1.4 Conclusions

In conclusion, quenching of PL of CdSe QDs may occur through electron transfer mechanism which depends on the LUMO energy levels of the analytes. Here, lower LUMO energy levels of analytes than the conduction band edge of CdSe QDs is important for an easy electron transfer.

1.5 References

[1]. L. Senesac, T. G. Thundat, Mater Today 11, 28, 2008.

[2]. E. R. Goldman, I. L. Medintz, J. L. Whitley, A. Hayhurst, A. R. Clapp, H. T. Uyeda, J. R. Deschamps, M. E. Lassman, H. Mattoussi, J. Am. Chem. Soc. 127, 6744, 2005.

[3]. S. Khatua, S. Goswami, S. Biswas, K. Tomar, H. Sekhar Jena, S. Konar, Chem. Mater. 27, 5349, 2015.

[4]. C. B. Murray, D. J. Norris, M. G. Bawendi, J. Am. Chem. Soc. 115, 8706, 1993.

[5]. H. Ostmark, S. Wallin, H. G. Ang, Propellants, Explos. Pyrotech. 37, 12, 2012.

[6]. C. Carrillo-Carrion, B. M. Simonet, M. Valcarcel, Anal. Chim. Acta 792, 93, 2013.

[7]. K. Zhang, H. Zhou, Q. Mei, S. Wang, G. Guan, R. Liu, J. Zhang, Z. Zhang, J. Am. Chem. Soc. 133, 8424, 2011

[8]. Z. A. Peng, X. Peng, J. Am. Chem. Soc. 123, 183, 2001.

[9]. J. C. Sanchez, A. G. DiPasquale, A. L. Rheingold, W. C. Trogler, Chem. Mater. 19, 6459, 2007.

[10]. D. Gao, Z. Wang, B. Liu, L. Ni, M. Wu, Z. Zhang, Anal. Chem. 80, 8545, 2008.

[11]. R. Tu, B. Liu, Z. Wang, D. Gao, F. Wang, Q. Fang, Z. Zhang, Anal. Chem. 80, 3458, 2008.

Part II.

EXPLOSIVE SENSOR PLATFORM BASED ON SILICON QUANTUM DOTS-EMBEDDED POROUS SILICON

Chapter One
Photoluminescent Porous Silicon for TNT Vapor Sensor

1.1 Introduction

Silicon Nanomaterials have been receiving ever increasing popularity in fields of researches because of its abundance, biocompatibility, and other intriguing features that other Nanomaterials do not possess. In particular, first reported by Canham [1], silicon quantum dots exhibit extraordinary phenomenon that emit visible photoluminescence (PL) due to their quantum confinement effect [2].

1.2 Experiments

1.2.1 Preparation of Photoluminescent PSi

N-type wafer (P-doped, 1.10 Ω cm, <100>-oriented, etched area ~10 cm2) was electrochemically etched under constant current density of 175 mA cm-2 for 320 sec. Platinum was used a cathode and the silicon wafer was used as an anode through hydrofluoric acid (HF) and ethanol (EtOH) in ratio of 1:1. The resulting wafer was rinsed with EtOH (99.9%) perier to drying under an argon atmosphere.

1.2.2 Synthesis of analytes

TNT, RDX, and PETN were prepared by following the method by Mario K.et al.4, Lange, Wen-Bin Y. et al[5], and K. et al.[6], respectively.TNT, RDX, and PETN are highly explosive and should be handled only in small quantities with extreme care.

1.2.3 Instrumentation and Data Acquisition

The anodization current was supplied by a Keithley 2420 high-precision current source meter. Steady-state PL spectra were obtained with an Ocean Optics S2000 spectrometer fitted with a fiber optic probe. The excitation source was a LED (λ_{max} = 460 nm) focused on the sample (at a 45^{o} angle to the normal of the surface) by means of a separate fiber. Light was

collected at a 90° angle to the incident light source with a fiber optic. Spectra were recorded with a CCD-detector in the wavelength range of 400-900 nm.

1.3 Results and Discussion

We investigated possibilities of PL Psi for explosive detection applications. PL PSi which of PL peaked at λmax= 650 nm was utilized for this sensing experiment. Since high explosive such as TNT is an excellent electron drawer, it is an efficient PL quencher. Naturally, we have employed PL quenching phenomenon for the sensing mechanism. As seen Figure 1, quenching of PL by TNT vapor was observed. Sensing vapor is particularly difficult, however it is crucial for the sensor to recognize low amount of the analyte in order to detect explosive traces.

After obtaining the successful TNT sensing result, sensing RDX and PETN vapor experiments were conducted. On the contrary, PL from PL PSi did not quench at all, as seen in Figure 2. The results can be explained by the vapor pressures of the analytes. TNT has vapor pressure of 7 parts per billion (ppb) when RDX and PETN have vapor pressures of 1.7 and 5.5 parts per trillion (ppt), respectively.

To investigate further if the vapor pressure is a key factor for sensing the analytes, TNT, RDX, and PETN in toluene solution were directly dropped on the PL PSi and then dried under argon atmosphere. The drop of TNT caused quenching of PL visibly by naked eyes. On the other hand, RDX and PETN did not affect the PL, as seen in Figure 3.

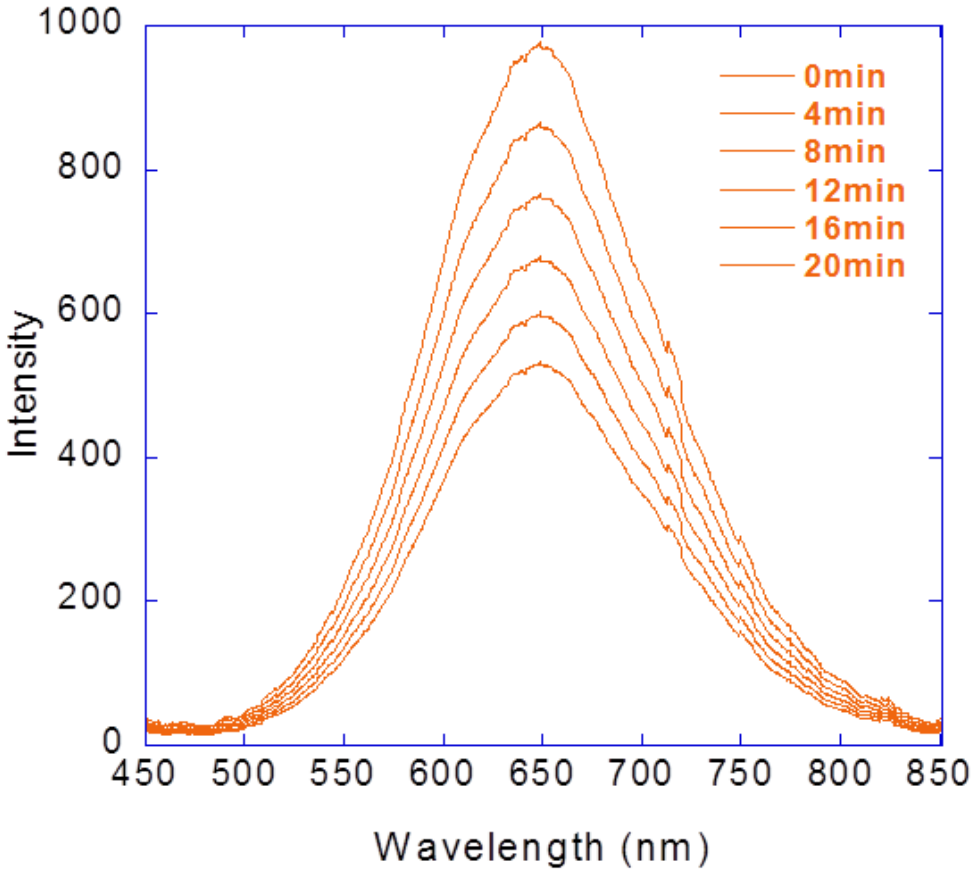

Figure. 1.1 TNT vapor saturated air was blown onto the PL PSi and PL was recorded every four minutes for 20 minutes

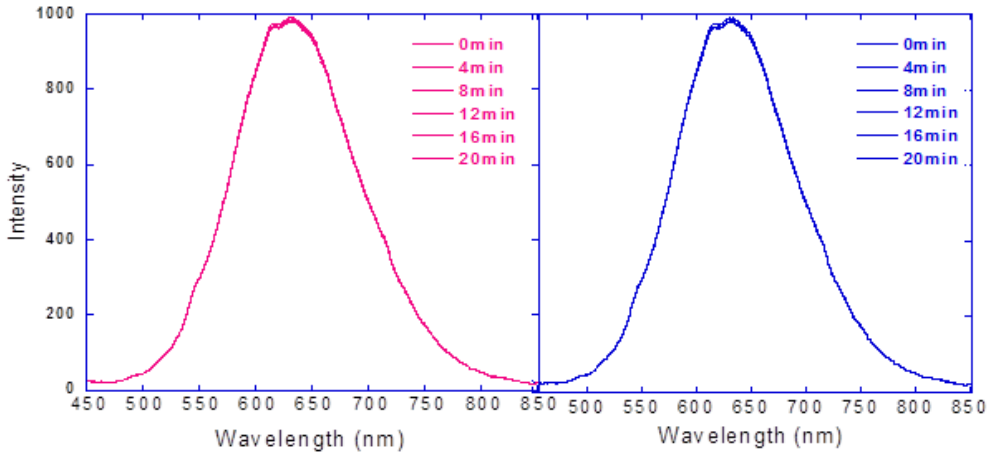

Figure. 1.2 RDX (a) and PETN (b) vapor saturated air was blown onto the PL PSi and PL was recorded every four minutes for 20 minutes

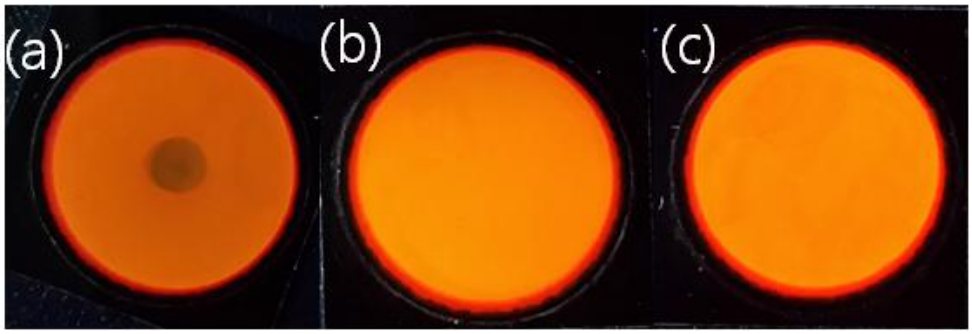

Figure. 1.3 TNT (a), RDX (b), and PETN (c) was dropped on PL PSi by amounts of 3.989×10^{-7} M, 4.092×10^{-7} M, and 1.79×10^{-7} M, respectively

The results suggested that the vapor pressure was not the only factor that mattered when sensing the analytes. It may be can be explained by looking at lowest occupied molecular orbital (LUMO) energy levels of the analytes. For PL PSi to donate electrons to an analyte easily, LUMO energy level of the analyte is preferred to be on a lower level. LUMO energy level of TNT, RDX, and PETN are -3.483, - 2.53, and -3.07 eV, respectively. The lowest lying LUMO energy level of TNT might have allowed for an easier and smoother electron transfer from PL PSi to TNT. Both vapor pressure and LUMO energy levels of the analytes play important roles, however LUMO energy level was the key factor in this sensing experiment.

1.4 Conclusions

PL PSi which of PL peaked at λmax= 650 nm was fabricated and utilized for this sensing of high explosives experiment. After obtaining the successful TNT sensing result, sensing of RDX and PETN vapor experiments were conducted which did not affect PL from PL PSi at all. May be because TNT has vapor pressure of 7 parts per billion (ppb) when RDX and PETN have vapor pressures of 1.7 and 5.5 parts per trillion (ppt), respectively. The result led us to conduct a direct contact sensing experiment. The drop of TNT caused quenching of PL visibly by naked eyes; however the experiments of RDX and PETN did not show any differences. It was possible that LUMO energy level was the key factor in this sensing experiment, since the lower lying LUMO energy level of TNT might have allowed for an easier and smoother electron transfer from PL PSi to TNT molecules.

1.5 References

[1]. L. T. Canham, Appl Phys Lett 57, 1046-1048 1990.

[2]. L. T. Canham, C. L. Reeves, D. O. King, P. J. Branfileld, J. G. Crabb, and M. C. L. Ward, Adv. Mater. 8, 850, 1996.

[3]. L. Vaccari, D. Canton, N. Zaffaroni, R. Villa, M. Tormen, and E. D. Fabrizio, Microelectron. Eng. 83, 1598, 2006.

[4]. Kroger, M.; Fels, G., J of Lab Com and Radioph 43 217-227, 2000E.

[5]. Yi, W.B. and Cai, C. J Hazard Mater 150, 3, 2008.

[6]. Lange, K., Koenig, A., Roegler, C., Seeling, A. and Lehmann, Bio & med chem lett 19, 3141-3144, 2009.

Chapter Two
Multi-Quantum Dot Embedded Silicon Particles for Ultra-Sensitive Explosives Detection

2.1 Introduction

Demands for effective explosive substance screening systems are growing due to ever increasing threats by misusage of explosives all over the world (1, 2). However, most of the common detection technics used for explosive at current security sensing areas, such as ion mobility spectrometry (IMS) and gas chromatography, are rather limited to satisfy the demands (3, 4). They are time consuming and require a large space to operate (5). Furthermore, other public areas (i.e. infrastructures of urban areas) are not completely safe from explosives-based threats and worstly, complicated to implement current explosives screening system (6, 7). To effectively screen explosives in controlled or uncontrolled environments, it requires small and inexpensive explosives trace sensors that are sufficiently sensitive and selective (8, 9). The strongest sensing platform candidates that are suitable to meet the current demand are chemical sensors such as metal organic framework (MOF), photoluminescent polymers, and quantum dots (QDs) based sensors; they have comparably easy detecting mechanism (10-12). Our focus was on porous silicon (PSi) as a possible solution to the problem. Researches on PSi have been gaining popularity over the years since Canham first reported a bright red-orange fluorescence from PSi (13). Various fields of researchers have

been paying increasing attention to PSi due to its intriguing features, such as efficient visible light emission, large specific surface area and highly tunable pore size (14, 15). By utilizing the traits of PSi, various kinds of sensing applications are studied ranging from DNA to volatile organic compounds (16-20). Owing to its simple fabrication process and high tunability, electrochemical etching of silicon wafer method is one of the most popular methods used by many researchers to obtain PSi (21, 22). Optimization of collecting and sensing analytes can be achieved by modulating the large surface area and capillary condensation effect that PSi possesses. Also visible photoluminescence (PL) from PSi allows an easy and simple sensing through energy-transfer mechanism. These advantages of PSi as a sensor are compacted in a reasonably small structure and they are inexpensive to fashion, thus capable of attaining current demand of mass deployment. Previously, a number of research articles on sensing explosives based on optical characteristics of PSi has been published by using electrochemically-etched silicon wafer (23, 24).

We wanted to lucubrate further and exploit its properties of optical communication, which enables wide range detection of explosives. E. Rehman and D. Al-Khursan have discovered that Double QD (DQD) structure possess rich possibilities in all-optical manipulation which is critical in optical communication applications (25). The two dots form a system configuration of two subsystems which construct subbands. The pumping field and coupling field induces transition between subbands of two quantum dots. The light wave fills the entire structure of the QD active region and interacts with all QDs in the structure. As a result, the total length of QD is increased and averaged. The averaged photon density is defined by equation (1) and averaged QD structure length, L, can obtain by equation (2).

$$s_i(z,t) = (s_i(t))_{in} \times \exp\left(\int_0^z (g_i - \alpha_{int})dz'\right) \quad (1)$$

$$s_i(t) = \frac{1}{L}(s_i(t))_{in} \times \int_0^L (g_i - \alpha_{int})dz') \quad (2)$$

In this study, we fabricated PSi particles of multiple QDs to study its morphology, optical characteristics, sensing efficiency, and detection mechanism through investigating detection of 2-Methyl-1,3,5-trinitrobenzene (TNT), 3-(nitrooxy)-2,2-bis[(nitrooxy)methyl]propylnitrat (PETN), 1,3,5-trinitroperhydro-1,3,5-triazine (RDX), and 2,3-dimethyl-2,3-dinitrobutane (DMNB) which are commonly found compounds in modern explosives and explosive taggants. In the real-world environment, it is imperative to detect explosive vapor trace. In order to test the non-contact vapor sensing, a portable detection device was designed and built to exhibit an example of a feasible real-world application.

2.2 Experiments

2.2.1 Preparation of Photoluminescent PSi

N-type wafer (P-doped, 1-10 Ω cm, <100>-oriented) was electrochemically etched under constant current density of 175 mA cm-2 for 320 sec. Platinum was used a cathode and the silicon wafer was used as an anode through hydrofluoric acid (HF) and ethanol (EtOH) in ratio of 1:1. The resulting wafer was rinsed with EtOH (99.9%) perier to drying under an argon atmosphere. The silicon particles then detached from the substrate and

suspended in toluene solution via ultra-sonication (800 W, 23 kHz custom designed by centralizing cores) method for 10 minutes.

As-prepared porous silicon sample was added to the vacuumed Schlenk flask and 1 mL of n-butyllithium was added by syringe. Then it was left for 3 hrs before removing the solution by syringe. The flask was cooled to in an acetone and dry ice bath prior to addition of 3 mL of trifluoroacetic acid. The flask was then allowed to return to room temperature. (The solutions above were purchased from Sigma-Aldrich and used without further purification.)

2.2.2 Instruments

Fluorescence lifetime was measured using a time-resolved fluorescence spectrophotometer (MicroTime-200, Picoquant, Germany). A single-mode pulsed diode laser (375 nm with a pulse width of ~240 ps and an average power of ~5 μW) was used as an excitation source. Time-correlated single-photon counting (TCSPC) technique was used to count emission photons to enable decay curve. Exponential fittings for the measured fluorescence decay curves were performed by the iterative least-squares deconvolution fitting method using the Symphotime software (version 5.3). Dynamic light scattering (DLS) measurement was conducted by employing a DLS-8000HL (Otsuka Electronics, Japan) with 10 mW He-Ne Laser (Max 30m W), photomultiplier tube detector, and silicon photodiode monitor detector. Electron paramagnetic resonance (EPR) was measured by a JES-FA200 (JEOL, USA) with X-band of 8.75 - 9.65 GHz, sensitivity of 7 x 109 spins/0.1 mT, and resolution of 2.35 μT or better. Absolute photoluminescence (PL) quantum yield (QY) was obtained by using a

Quantaurus-QY Absolute PL quantum yield spectrometer C11347-11 (Hamamatsu, Japan) with of 150 W xenon monochromatic light source, multichannel Czerny-Turner type spectroscope, and 3.3 inch spectralon integrating sphere. To measure specific surface area and pore sizes, Brunauer-Emmett-Teller (BET) and Barrett-Joyner-Halenda (BJH) analyses were employed by using ASAP 2020 (Micromeritics, USA) with pressure measure resolution of 0.000001 mmHg. PL of electro-chemically etched porous silicon (before ultra-sonication) was measured by USB2000 (Ocean Optics, USA) and the LED excitation source (λmax = 400 nm) was focused on the sample (at a 45O angle to the normal of the surface) by means of a separate fiber. PL when the sample particles are suspended in solution,was obtained by LS 55 fluorescence spectrometer (PerkinElmer, USA) with pulsed Xenon flash lamp at line frequency of 50 or 60 Hz and R928 photomultiplier. UV-Vis absorption spectra were acquired by UV-2401 (Shimadzu Corporation, Japan) with grating double monochromator, photomultiplier type detector, and 150 Ø integrating sphere. Fourier transform infrared spectroscopy (FT-IR) spectra were obtained by using Nicolet 5700 (Thermo Electron Corporation, USA) with DlaTGS w/KBr detector and Ge-on-KBr beamsplitter. X-ray photoelectron spectroscopy (XPS) measurements were conducted by using ESCALAB 250 (Thermo Fisher, USA) with monochromated Al-Ká (1486.6 eV) energy source. High resolution transmission electron microscope (HR-TEM) images were obtained by JEM-2100F (JEOL, USA) with point resolution of 0.19 nm and line resolution of 0.10 nm. Field emission scanning electron microscope (FE-SEM) images were acquired by Hitachi S-4700 (Hitachi, Japan) with cold field emission type electron gun and column system electron gun and 0.5 to 30 kV accelerating voltage.

2.3 Results and Discussion

Luminescent PSi is known to be highly susceptible to native oxidation process at room temperature and in ambient air, leading to decrease in quantum yield (26). This phenomenon can have negative effects on durability and sensitivity as a sensor. Therefore, it is important to passivate the surface of the nanoparticles to prevent or slow down the native oxidation process. Song, J. H. and Sailor, M. J. reported a surface passivation method without significantly compromising PL intensity (27). Employing a minor modification to the passivation method, the fabricated luminescent PSi showed comparably good resistance against the native oxidation process. For a comparison study between the pre- and post- surface passivation samples, the absolute quantum yield (QY) was measured every 5 minutes for one hour (shown in Table 2.1 and Fig. 2.1). During the experiment, both samples were constantly exposed to ambient air in room temperature. The decrease in PL intensity of pre-passivated sample was assumed to be caused by the native oxidation process, which was accelerated by photo-bleaching by UV light source during the Absolute Quantum Yield measurement.

Table 2.1 Absolute Quantum Yields of both before (Green) and after (Blue) the passivation by Alkyl group were measured every 5 minutes for 1 hour.

Time	Si-H	Si-R
0min	46.3 %	27.5 %
5min	42.5 %	27.4 %
10min	39.5 %	27.1 %
15min	36.1 %	27.5 %
20min	33.1 %	27.6 %
25min	31.4 %	27.7 %
30min	27.7 %	27.8 %
35min	25.4 %	27.1 %
40min	23.2 %	27.5 %
45min	21.9 %	27.6 %
50min	19.8 %	27.6 %
55min	17.4 %	27.6 %
60min	15.4 %	27.7 %

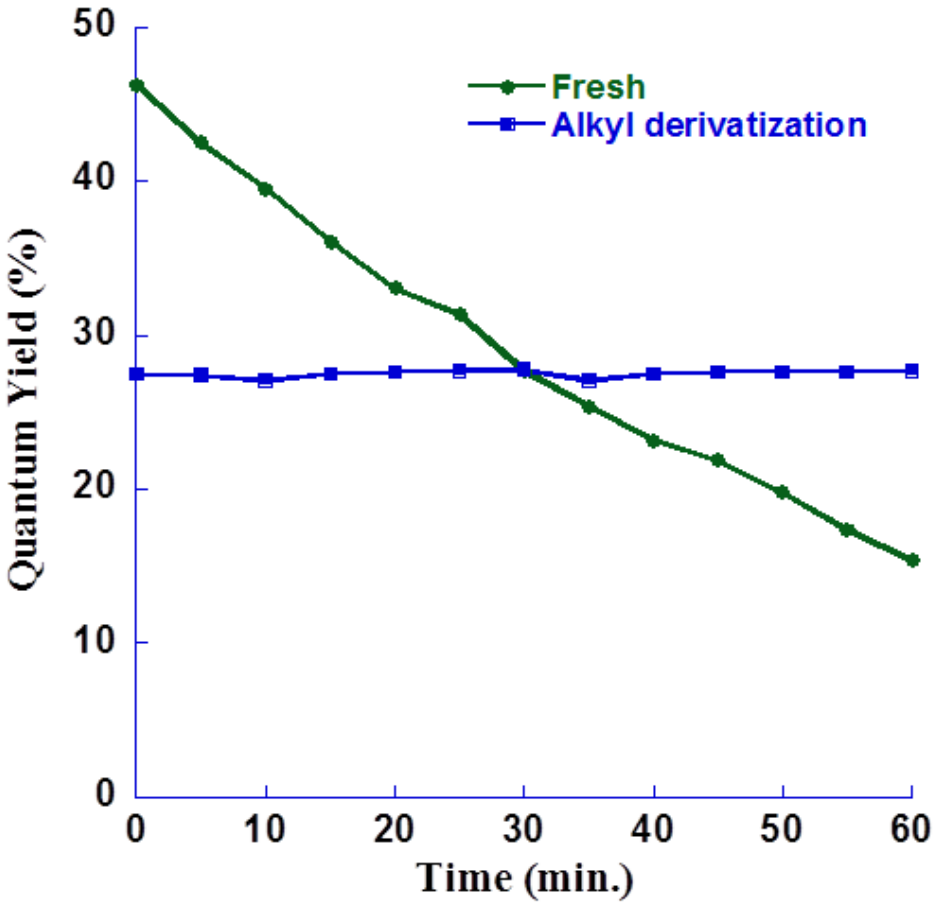

Fig 2.1 Plot for Table 2.1 showing the stability of PL from passivated sample compare to PL from non-passivated sample

The surface passivation was characterized by Energy-dispersive X-ray spectroscopy (EDS) analyses. Figure 2.2 exhibits atomic composition of 50.38% C and the rest Si. Also, Fig. 2.3 shows FT-IR measurement of new peaks, Si-C bond and υ(CH3), at 781 cm-1 and 2850 cm-1, respectively. The result indicates the formation of a new species of phenylacetylide group. Energy binding study was done by X-ray photoelectron spectroscopy (XPS) analysis; the result is indicated in 2.4.

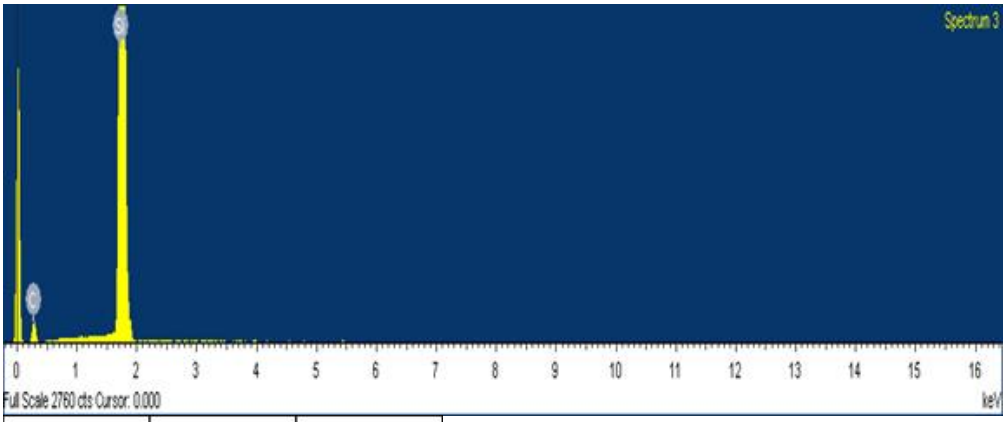

Element	Weight%	Atomic%
C	30.28	50.38
Si	69.72	49.62
Totals	100.00	

Fig 2.2 Energy-dispersive X-ray spectroscopy (EDS) showing as-fabricated sample's elements are consisted of Si and C

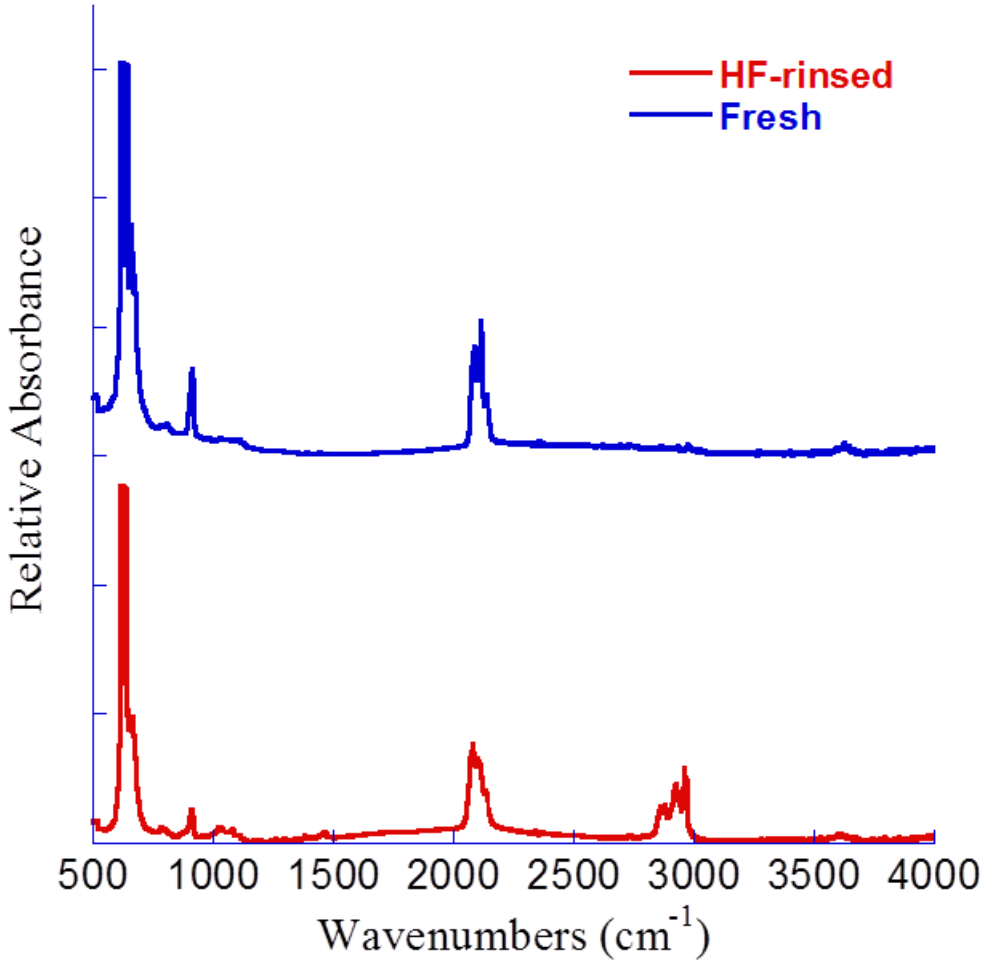

Fig 2.3 FTIR spectra of before (top) and after (bottom) alkyl-terminated as-fabricated sample

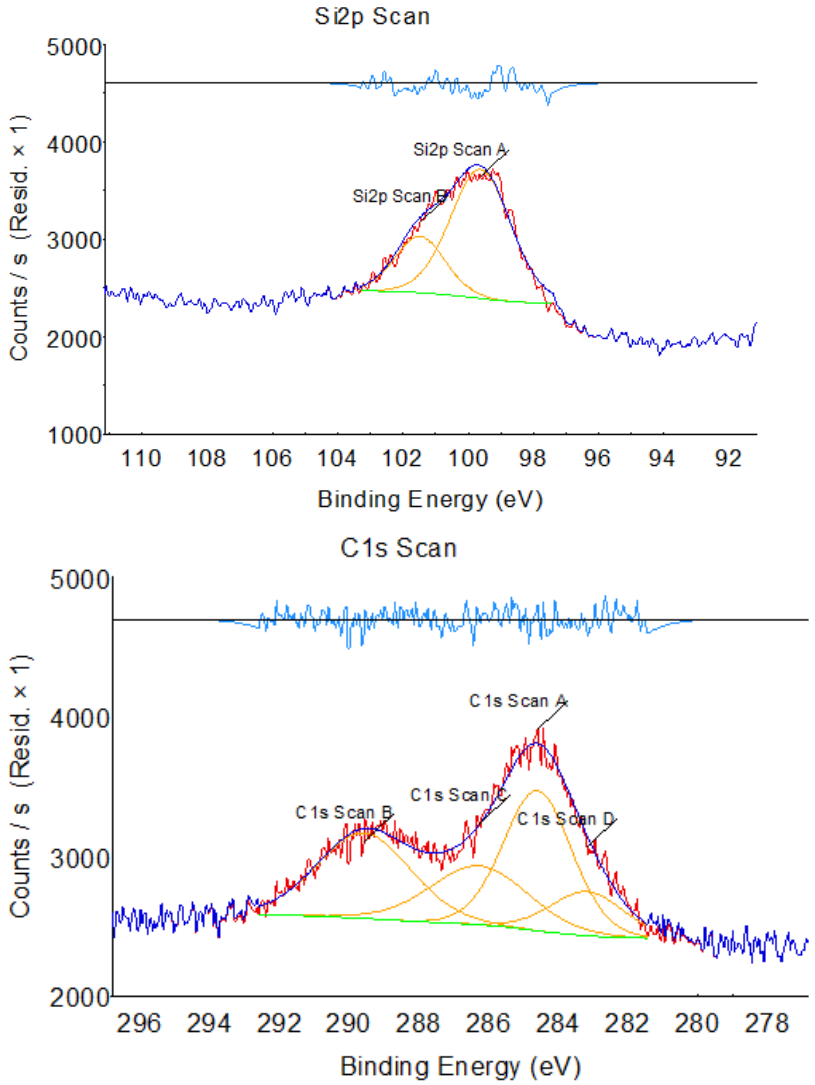

Fig 2.4 X-ray photoelectron spectroscopy (XPS) spectra of Si2P (top) and C1s (bottom) of as-fabricated silicon particle

UV absorption and PL spectra peaks at λmax = 310 nm and λmax = 630 nm, respectably (shown in Fig. 2.5). The passivation caused PL peak to red-shift by 23 nm (shown in Fig. 2.6), due to the narrower bandgap resulted from the surrounding alkyl groups (28). Scanning electron microscope (SEM) and transmission electron microscope (TEM) showed evenly distributed amorphous nanoparticles and silicon lattice structure as depicted in Fig. 2.7. The particle sizes were analyzed by dynamic light scattering (DLS) measurement. The DLS measurement shows that the diameters of particles were varied approximately from 50 to 60 nm (shown in Fig. 2.8).

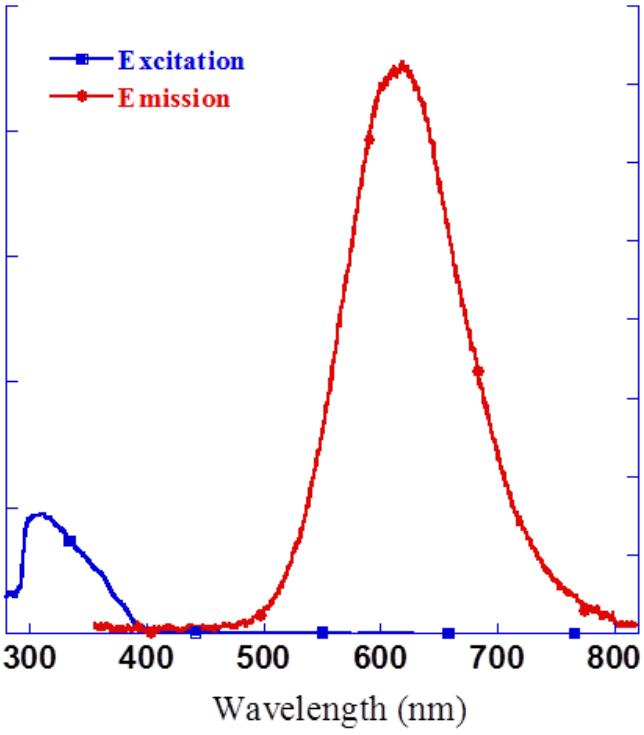

Fig 2.5 UV absorption band and PL spectra of as-fabricated silicon particles

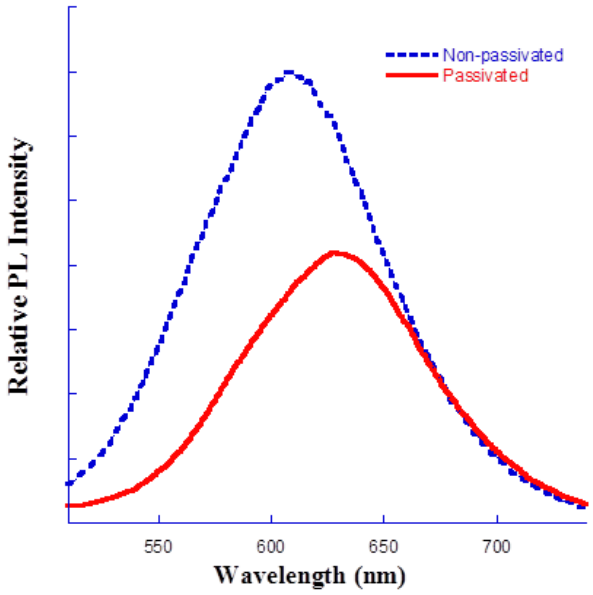

Fig 2.6 PL spectra of before (dotted blue) and after (solid red) alkyl-terminated of silicon particles

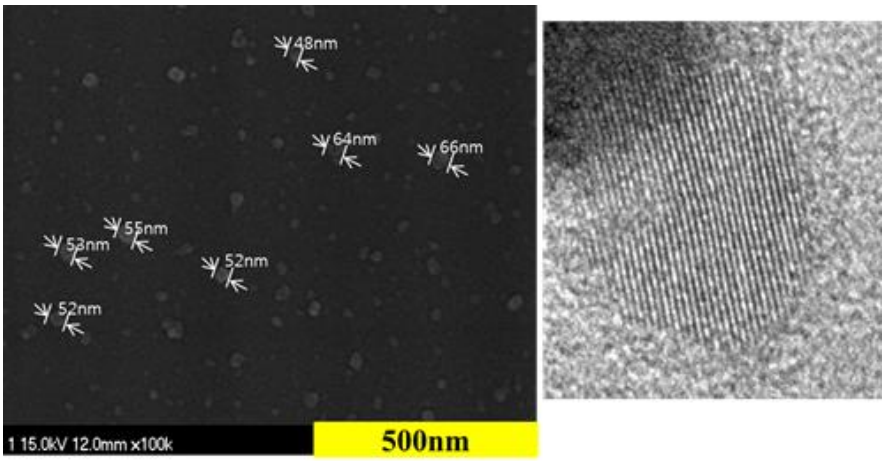

Fig 2.7 SEM image (left) of as-prepared sample and magnified image by HR-TEM showing lattice structures of silicon nanoparticle (right)

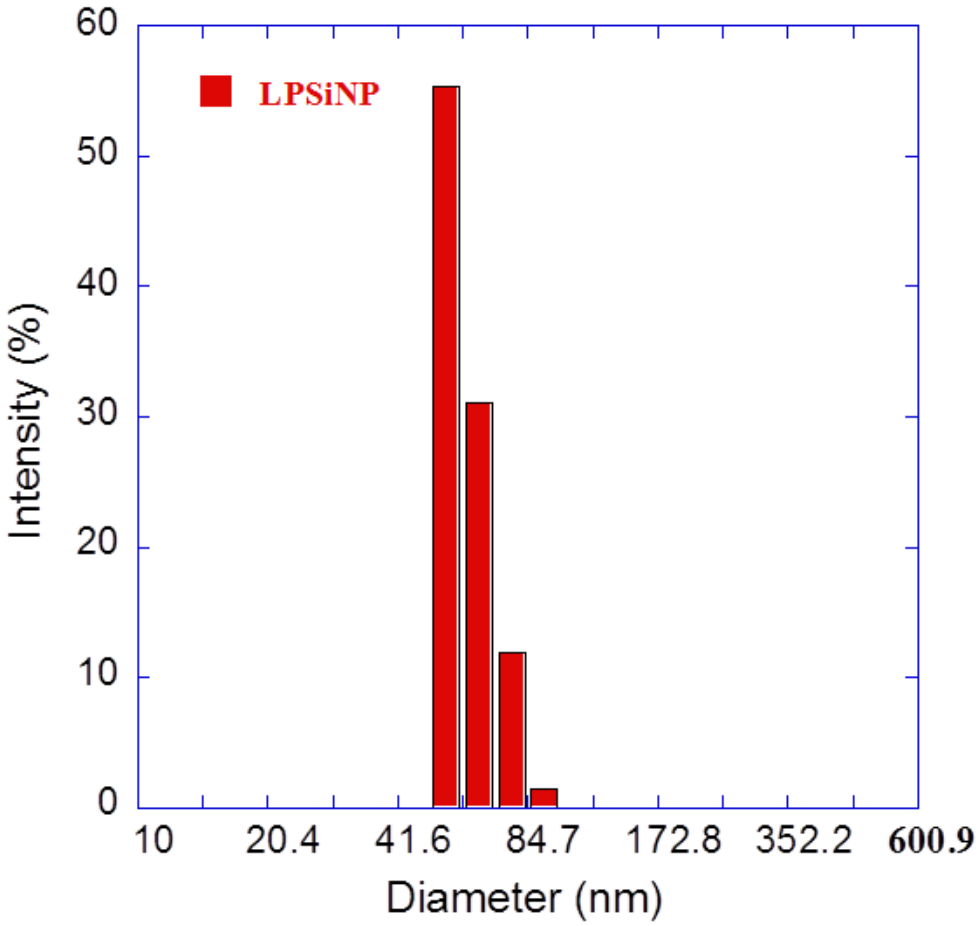

Diameter (nm)	49.7 (nm)	59.3 (nm)	70.9 (nm)	84.7 (nm)
Intensity (%)	55.39 %	31.04 %	11.9 %	1.38 %

Fig 2.8 Dynamic light scattering (DLS) measurement that showing the majority particles' diameters of the sample are approximately between 50 to 60 nm

We employed as-fabricated porous silicon (PSi) as a sensing platform for detecting explosives such as TNT, PETN, RDX, and an explosives taggent DMNB which are commonly found compounds in modern days. Sensing experiment was conducted by introducing relatively low amount of analyte to the prepared samples and PL quenching spectra was recorded after each addition of 0.43×10^{-6} M, 0.31×10^{-6} M, 0.45×10^{-6} M, and 0.56×10^{-6} M of TNT, PETN, and RDX, respectively, as displayed in Fig. 2.9.

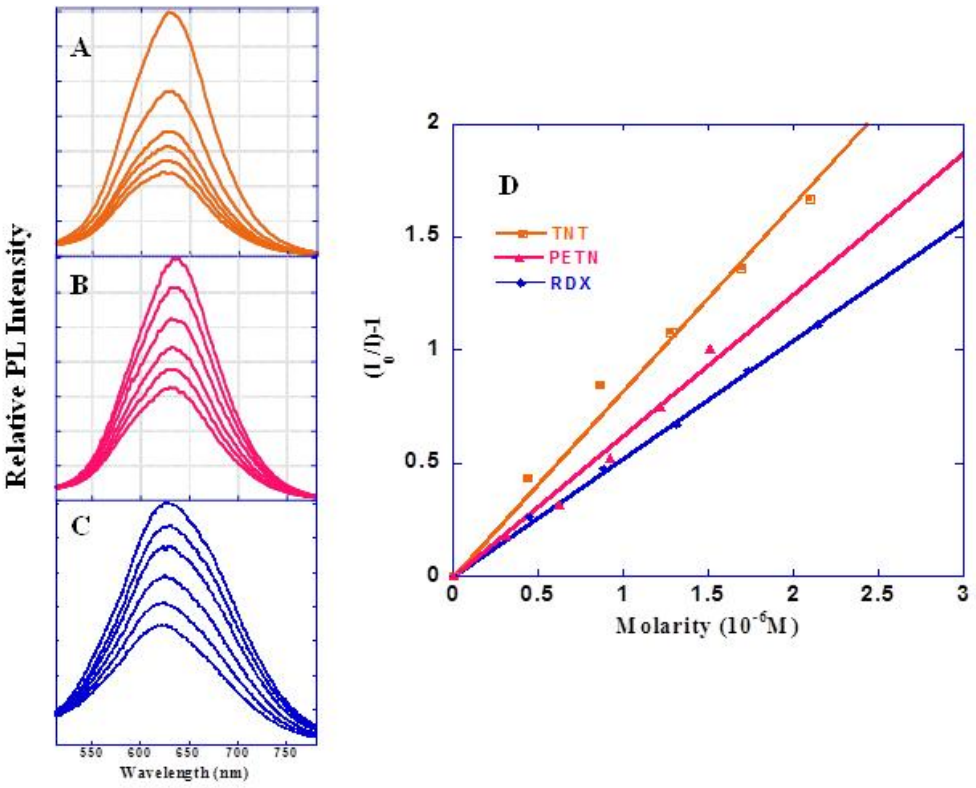

Fig 2.9 PL quenching spectra of the sample recorded after each addition of 0.43×10^{-6} M, 0.31×10^{-6} M, and 0.45×10^{-6} M TNT (A), PETN (B), and RDX (C), respectively, in solution and the Stern-Volmer plots for quenching efficiency of MQED silicon particles with introduction of TNT, PETN, and RDX (D)

PL of the sample quenched significantly upon each addition of the analytes. To study the PL quenching behavior by energy-transfer, electron paramagnetic resonance (EPR) analysis was employed and the result showed the decrease in radicals when the sample was mixed with TNT (shown in Fig. 2.10). Also lifetimes of PL as a function of TNT, PETN, RDX, and DMNB were measured (results shown in Fig. 11). There was no change in the mean lifetime observed at each addition of analytes, indicating the dominant process of static quenching.

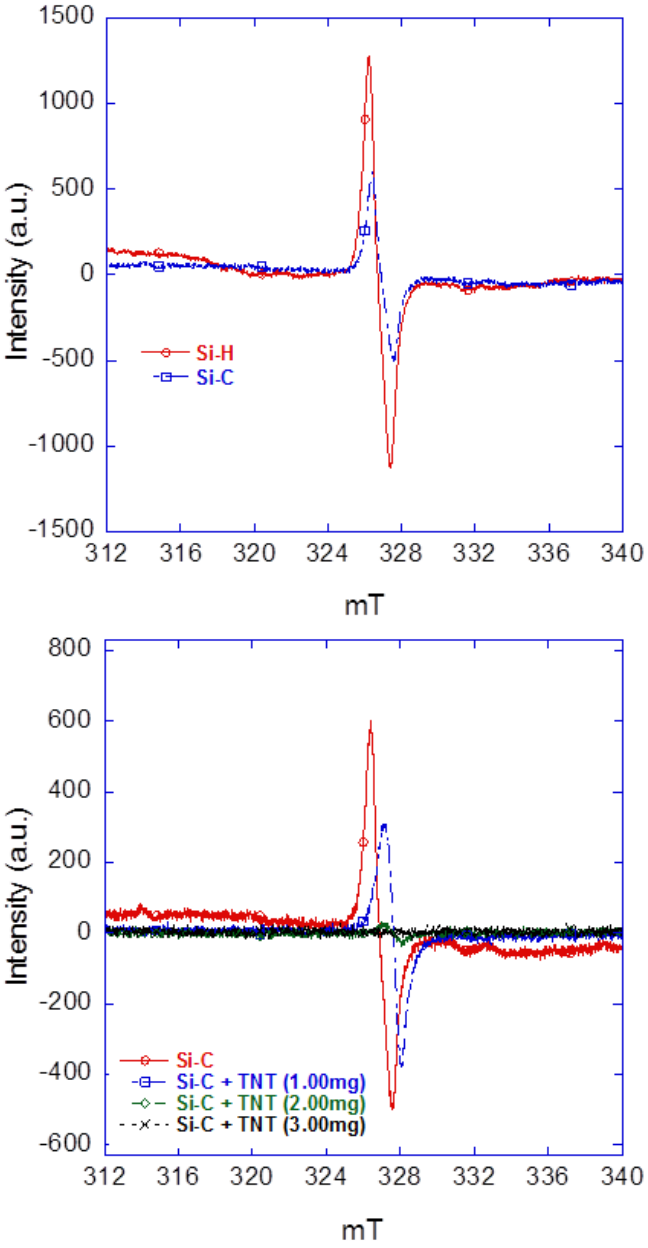

Fig 2.10 Electron spin resonance (EPR) measurement that showing radical intensities of as-fabricated silicon particles before and after the passivation (top), also with and without increasing amount of TNT (bottom)

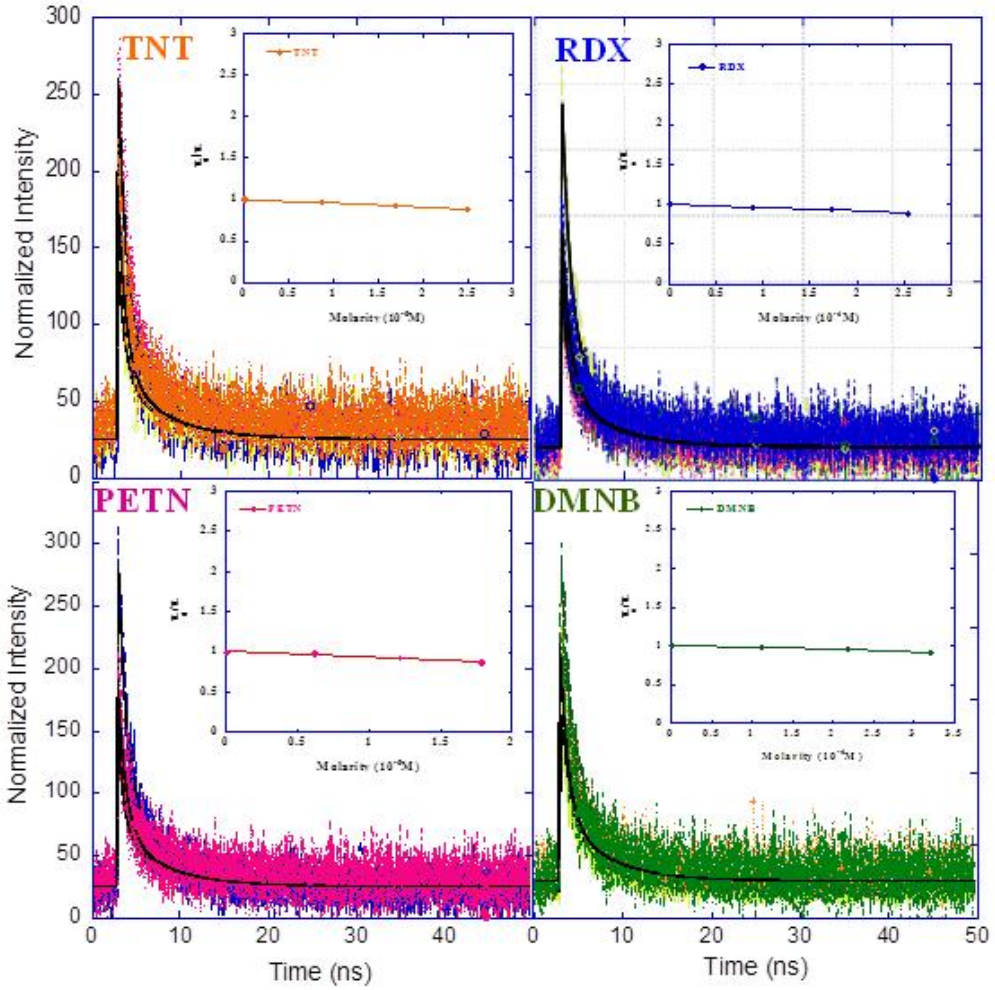

Fig 2.11 Fluorescence decays of as-fabricated silicon particles for different concentrations of analytes (3 additions of 0.44 × 10-6 M, 0.31 × 10-6 M, 0.45 × 10-6 M, and 0.56 × 10-6 M of TNT, PETN, RDX, and DMNB, respectively); the plots of fluorescence lifetime ($\tau o/\tau$) (shown in the inset) indicate its' independence of the amount of analytes added

For studying the sensitivity, Stern-Volmer relationship is a useful tool to analyze the sensing efficiency and to make comparison between the analytes. Stern-Volmer constant (K_{sv}) is derived by the equation (3),

$$\frac{I_f^o}{I_f} = 1 + K_{sv} \cdot [Q] \qquad (3)$$

where I_f^o is the intensity without a quencher, I_f is the intensity with a quencher, [Q] is the concentration of the quencher, and K_{sv} is the quencher rate coefficient. By substituting the result from Fig. 4 to equation (1), Stern-Volmer constants for TNT was K_{sv} = 822,950 the highest followed by PETN K_{sv} = 623,370 and RDX K_{sv} = 521,750. The sensing experiment result demonstrated the superiority of high efficiency in quenching of PL to other sensing materials. Gao et al. reported K_{sv} = 9038 for TNT and K_{sv} = 2011 for RDX based on dye-modified silica nanoparticles, as well as Zyryanov et al. reported Ksv = 3300 for TNT based on 1,4-diarylpentiptycene (29, 30). The result also suggested a potential for a sensor of multiple-explosive since the quenching of PL occurred with every analyte we tested.

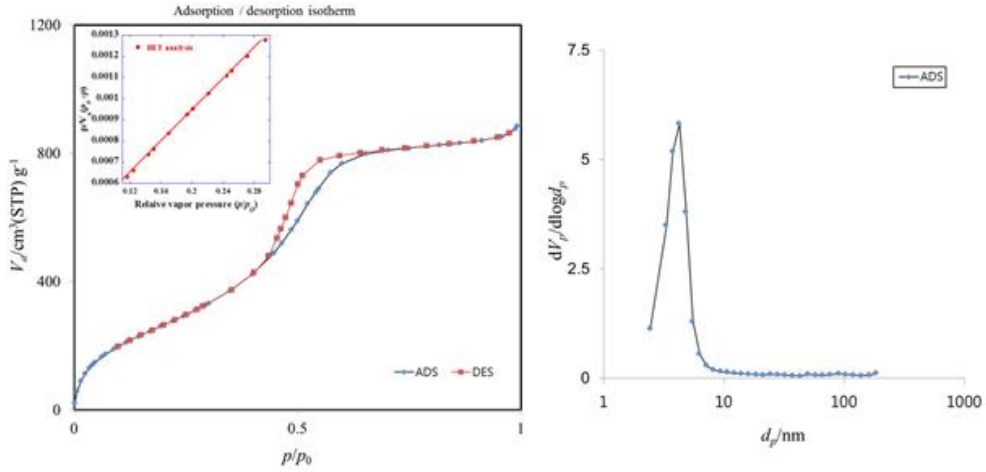

Fig 2.12 Adsorption and desorption isotherm (left) and BJH analysis for the particle size (right) of MQDE silicon particles

Such results could be rationalized by the characteristics of PSi. The porous morphology of nanoparticles is interpreted as the large specific surface area and capillary condensation effect. These effects part take as crucial roles in sensing materials as the probability of collecting samples increases sharply due to the increased surface area of the collecting site. Figure 2.12 depicts the gas adsorption/desorption spectra analyzed by Brunauer, Emmett, Teller (BET) and Barrett-Joyner-Halenda (BJH). The pore size distributions of the sample confirmed significantly high porosity of micropores with high specific surface area which was 1056.4 m^2/g; close to the highest specific surface area of PSi reported (31). It is worth noting that p-type silicon wafer is usually preferred when the aim is to obtain micropores and a high surface area rather than n-type. P-type silicon wafer is known to yield more refined and evenly distributed pores during the anodization (14). However, as-prepared PSi particles became more complex on the surface area after the

passivation. We believe that the passivation may have contributed to the very high specific surface area. Since the sensitivity of the sensor largely depends on the ability of collecting samples, such high Stern-Volmer constant values may have been inevitable.

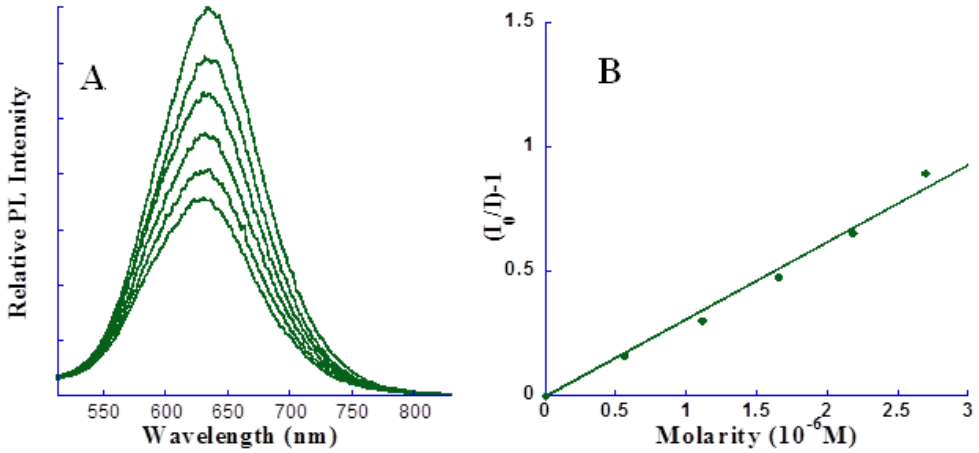

Fig 2.13 PL quenching spectra of the sample recorded after each addition of 0.56×10^{-6} M of DMNB in solution (A) and the Stern-Volmer plot (B)

On the other hand, other various sensing platforms have porous structure similar to PSi (32, 33). The porous structure itself does not fully explain the surprisingly high sensitivity, as well as, the successful detection of DMNB (DMNB sensing experiment was conducted by the same fashion as the experiment with other analytes; 0.56×10^{-6} M of DMNB was added five times to as-fabricated silicon particle solution) as shown in Fig. 2.13. Quenching of PL by DMNB was unexpected; DMNB was known to be extremely difficult to detect. DMNB has high vapor pressure which eases canines to detect, on the other hand a high LUMO energy level can be an obstacle to detect by the energy transfer sensing method. Thus, one requires

more than a porous structure and a large specific surface area; they only enhance collection of analytes (34). As aforementioned, detection of DMNB by energy transferring was proven particularly difficult, because in order to achieve an effective energy migration, an electron donor must have a higher LUMO energy level than DMNB's LUMO energy. We demonstrated in our recent study that blue silicon QDs with higher LUMO energy level detected DMNB, however cadmium selenide (CdSe) QDs with lower LUMO energy level than that of DMNB failed to detect (35). Energy band gaps of QDs have unique properties. The band gaps depend on the size of QDs. As the size of QDs decreases the energy band gap is widened causing the centroid of PL spectra to blue-shift (36). Although the majority sizes of as-fabricated silicon particles' QDs display the centroid at 640 nm in PL spectra, a comparably small group of smaller sized QDs, which emit shorter wavelength, ought to exist as well. The forming of multi-sized QDs is assumed to be formed from the process of electrochemical etching that branched into silicon matrix as 1st order pore, 2nd order pore, and so on leading to different rates of forming QDs. Since smaller QDs have wider band gaps with higher LUMO energy levels, they have the higher possibility of energy transfer to DMNB molecules. However, albeit with the existence of smaller QDs, sensing experiment of DMNB should have yielded extremely low or no result at all because, the PL spectra suggested that the sample contained small population of smaller QDs. However, Fig 4 (b) depicts not only a successful detection but also a surprisingly high sensitivity with Ksv = 310,600 compared to other sensing platforms (34, 37). This phenomenon may be caused by the same inter-chain energy migration that is seen from other

chemo sensors such as conjugated polymers (38). The conjugated polymers show enhanced sensing ability in solid conjugated form than suspended in solution. The solid conjugated form creates better energy interaction between the polymers. The same effect could be at work in as-prepared multi quantum dots embedded (MQDE) silicon particle. PSi detached from substrates by ultra-sonication, it then was divided into nanoparticles and each of them carry various sizes of QDs. QDs within the same nanoparticle, are connected and interacted each other by intra-particle interaction effect (IPIE). The size of each particle is small enough to allow IPIE to occur, providing energy migration pathways for excitons. Consequently, one QD's behavior affects the surrounding QDs, much like in amplifying conjugated polymer and Metal Organic Framework (MOF) in aggregated state (39). Thus, PL quenching of one single QD causes other surrounding QDs within the same particle to follow suits. IPIE of MQDE silicon particle's energy band gaps could have interaction of electron transfer from a wider band gap. The interaction could affect the majority QDs with narrower energy band gaps. Comparison between single-sized red quantum dots and MQDE silicon particles conveys the possible state of energy band gaps. The limitations of energy transfer set by analyte's higher LUMO energy level does not apply to MQDE silicon particles since a perturbation in wider energy band gap by an analyte with higher LUMO energy levels such as DMNB affect the entire system of the multi energy band gap.

To test our hypothesis that MQDE silicon particles have IPIE enforced by their small sizes, an explosive-vapor sensing test by undetached (non-ultra-sonicated) luminescent PSi was carried out. A small PL quenching

of the undetached PS occurred only when TNT vapor was introduced, whereas PETN, REX, and DMNB vapors either did not affect PL or minimally affected (Fig. 1.14). The difference in sensitivity between undetached and dethatched PS could be seen clearly. One of the reasons that could be assumed is that the exposed surface area of undetached luminescent PSi to the analytes was smaller than the silicon particles' 3 dimensional structures. Another reason is that when PSi layer is attached to its substrate, bulk silicon, IPIE may have been interrupted. The energy could not be captured in a small container that prevented interaction between QDs.

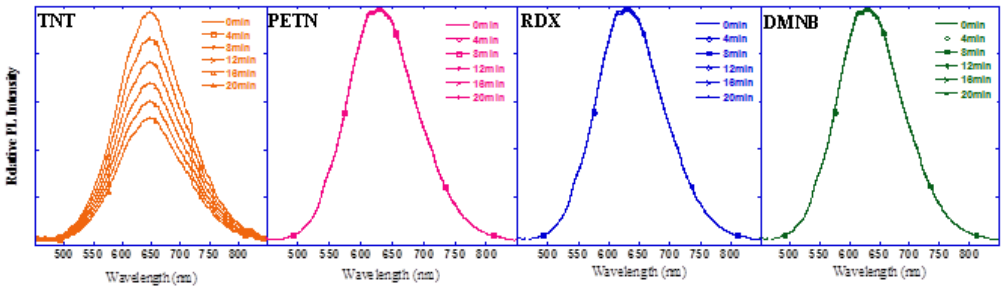

Fig 2.14 Quenching PL of porous silicon on substrate without detaching from silicon wafer substrate was observed under constant stream of TNT, PETN, RDX, and DMNB vapor

Explosive vapor sensing experiment was conducted by using a custom designed device to assess the feasibility for real-world application. As depicted in Fig. 2.15, MQDE silicon particles were drop-casted on a glass

lens that was illuminated by a UV light excitation source. PL from MQDE silicon particles was continuously monitored through a complementary metal-oxide-semiconductor (CMOS). In order to prevent the UV light directly reaching the CMOS, an optical filter was placed between the CMOS and MQDE silicon particle coated lens. The device was inserted into the airtight chamber where analyte of interest was left overnight to create a fully saturated atmosphere. The chamber door was kept closed during the sensing experiment. After 20sec of the exposure to the analyte, the device was taken out from the chamber to the ambient air atmosphere to observe the PL recovery of the sensor. The process was repeated three times to test the reversibility for continuous and rapid detection.

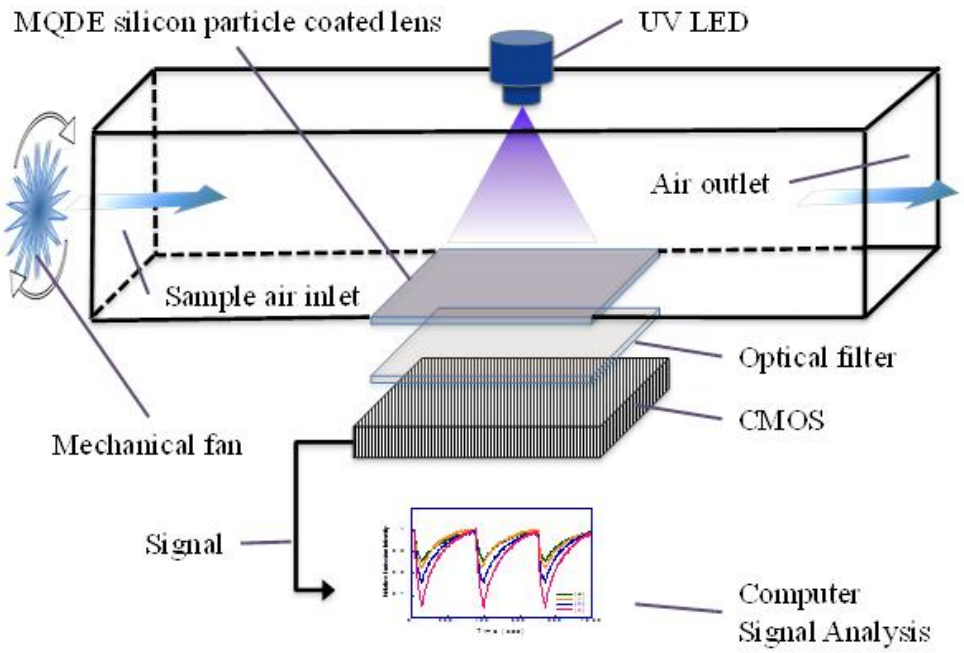

Fig 2.15 Schematic for vapor sensing device

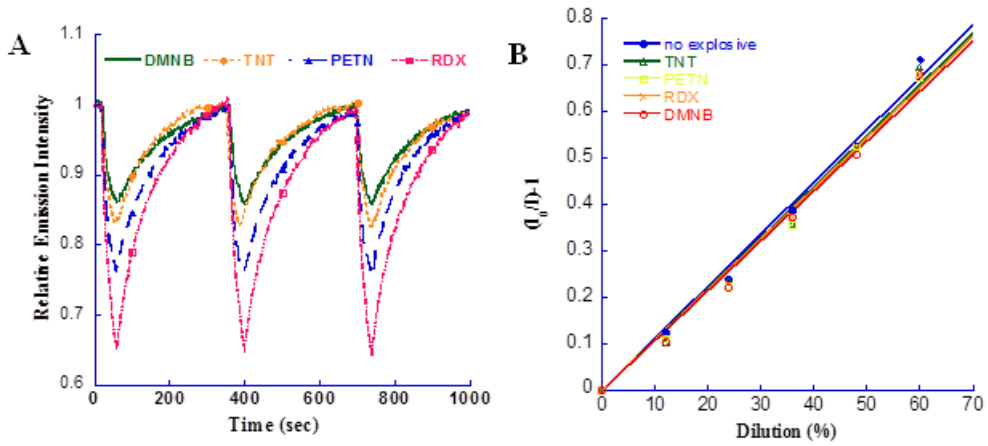

Fig 2.16 Result of vapor sensing by the device (A) and PL recovery study through diluting MQDE silicon particles in solution with and without analytes (B)

As seen in Fig. 2.16 (A), when vapor of the analytes contacted the sensor's membrane, the PL quenched instantly and subsequently fully recovered after 5min. Complete recovery of PL indicated that the passivation of MQDE silicon particles by alkyl group successfully prevented oxidation process that leads to decrease in PL. Without the passivation, PL would decrease by both oxidation process and vapor of an analyte and recover only by a small portion (shown in Fig. S11). To fully test the PL recovery of MQDE silicon particle after quenched by analytes, MQDE silicon particles in solution with and without analytes were diluted with increased amount of solvent. As depicted in Fig. 2.16 (B), MQDE silicon particles' PL of both with and without analytes decreased at the same rate. This indicated full recovery of PL, which is coherent with the vapor test result.

2.4 Conclusions

To summarize, Si QDs obtained by the reaction of magnesium silicide with ethylenediamine dihydrochloride from our previous study were utilized to explore a possibility of detecting an explosive taggant as well as to understand the sensing mechanism. Two different emission bands of Si QDs were synthesized at a peak wavelength of λmax = 460 (blue) and λmax = 520 nm (green). DNMB was successfully detected using blue luminescent Si QD solution with comparably good sensitivity, and analyzed by the Stern.Volmer relationship. The comparison result showed that Si QDs with a high lying conduction band have better sensitivity in sensing DMNB compared to CdSe QDs. For an easy electron transfer, the sensory system requires to have a matching conduction band edge with the LUMO energy level of the analyte.

2.5 References

[1] A. A. Adams, P. T. Charles, J. R. Deschamps, A. W. Kusterbeck, Anal. Chem. 83, 8411-8419, 2011.

[2] M. Tonouchi, Nature Photonics, 1, 97-105 2007.

[3] Z. Gong et al. ACS Appl Mater Interfaces, 6, 21931-21937 2014.

[4] B. C. Giordano et al., Anal Chem 88, 3747-3753 2016.

[5] L. Senesac, T. G. Thundat, Nanosensors for trace explosive detection. Mater Today 11, 28-36 2008.

[6] A. Hakonen, P. O. Andersson, M. Stenbaek Schmidt, T. Rindzevicius, M. Kall, Anal Chim Acta 893, 1-13 2015.

[7] E. Windsor et al., Anal Chem 82, 8519-8524 2010.

[8] C. Wang et al., Sci Rep 6, 25015 2016.

[9] J. Qu, Y. Ge, B. Zu, Y. Li, X. Dou, Small 12, 1369-1377 2016.

[10] S. Pramanik, C. Zheng, X. Zhang, T. J. Emge, J. Li, J Am Chem Soc 133, 4153-4155 2011.

[11] H. Sohn, M. J. Sailor, D. Magde, W. C. Trogler, J Am Chem Soc 125, 3821-3830 2003.

[12] C. Carrillo-Carrion, B. M. Simonet, M. Valcarcel, Anal Chim Acta 792, 93-100 2013.

[13] L. T. Canham, Applied Physics Letters 57, 1046-1048 1990.

[14] L. Canham, Handbook of Porous Silicon. 2014.

[15] G. Korotcenkov, Structure and Surface Modification of Porous Silicon. 373-384 2014.

[16] Y. Y. Li et al., Science 299, 2045-2047 2003.

[17] B. Cho, S.-G. Lee, H.-G. Woo, H. Sohn, Journal of Nanoscience and Nanotechnology 14, 5844-5848 2014.

[18] H. Zhang, L. Lin, D. Liu, Q. Chen, J. Wu, Anal Chim Acta 953, 71-78 2017.

[19] C. Pacholski, C. Yu, G. M. Miskelly, D. Godin, M. J. Sailor, J Am Chem Soc 128, 4250-4252 2006.

[20] C. Chiappini et al., Adv Mater 27, 5147-5152 2015.

[21] M. Ge, J. Rong, X. Fang, C. Zhou, Nano Lett 12, 2318-2323 2012.

[22] Z. Shen et al., Anal Chem 73, 612-619 2001.

[23] I. A. Levitsky, W. B. Euler, N. Tokranova, A. Rose, App Phy Lett 90, 2007.

[24] J. H. Song, M. J. Sailor, J Am Chem Soc, 119, 7381-7385 1997.

[25] E. Rehman, A. H. Al-Khursan, Appl Opt 55, 7337-7344 2016.

[26] Z. Ding et al., Science 296, 1293-1297 2002.

[27] J. H. Song, M. J. Sailor, Inorg Chem 38, 1498-1503 1999.

[28] M. P. Stewart, J. M. Buriak, 37, 3257-3260 1998.

[29] D. Gao et al., Anal Chem 80, 8545-8553 2008.

[30] G. V. Zyryanov, M. A. Palacios, P. Anzenbacher, Jr., Org Lett 10, 3681-3684 2008.

[31] A. Loni, L. T. Canham, T. Defforge, G. Gautier, Ecs J Solid State Sc 4, P289-P292 2015.

[32] T. Naddo et al., J Am Chem Soc 129, 6978-6979 2007.

[33] S. J. Toal, W. C. Trogler, J Mater Chem 16, 2871-2883 2006.

[34] S. W. Thomas, 3rd, J. P. Amara, R. E. Bjork, T. M. Swager, Chem Comm, 4572-4574 2005.

[35] J. S. Kim, B. Cho, S. G. Cho, H. Sohn, Chem Comm 52, 8207-8210 2016.

[36] A. P. Alivisatos, Science 271, 933-937 1996.

[37] M. E. Germain, T. R. Vargo, P. G. Khalifah, M. J. Knapp, Inorg Chem 46, 4422-4429 2007.

[38] S. W. Thomas, 3rd, G. D. Joly, T. M. Swager, Chem Rev 107, 1339-1386 2007.

[39] A. Lan et al., Angew Chem Int Ed Engl 48, 2334-2338 2009.

Appendices

Appendix
Curriculum Vitae

Educations (학위)

Ph. D. **2014. 09. ~ 2018. 02.** Carbon Materials, Chosun University
Research Advisor : **Prof. Honglae Sohn**
Thesis Title : **"Extra Sensitive Silicon Quantum Dots-embedded Porous Silicon Nanoparticles"**

B. S. **2010. 09. ~ 2014. 07.** Computer Science, Beijing Institute of Technology

Publications (논문게재)

SCI Journals (국제전문학술지)

1. "Detection of PETN and RDX Based on CdSe Quantum Dots", J-S. Kim, B. Cho, S-G. Cho and H. Sohn, Bulletin of the Korean Chemical Society, 2016, 37 (6), 789-790.

2. "Silicon quantum dot sensors for an explosive taggant, 2,3-dimethyl-2,3-dinitrobutane(DMNB)", J-S. Kim, B. Cho, S-G. Cho and H. Sohn, Chemical Communications, 2016, 52 (53), 8171-8322.

Oversea Journals (국외학술지게재논문)

1. "Photoluminescent Porous Silicon for TNT Vapor Sensor", J-S. Kim, B. Cho, S-G. Cho and H. Sohn, Biomirror, 2016, 7 (01), 1-4.

Awards (수상)

1. 제 4회 한국실리콘학회 우수포스터 발표상 (2015. 02. 12)
   "Investigation of Photoluminescence Efficiency of Silole-Capped Silicon Quantum Dots Based for Sensing Applications "

2. 18th International Symposium on Silicon Chemistry (ISOS XVIII) in conjunction with the 6th Asian Silicon Symposium (ASiS-6) 우수포스터 발표상 (2017. 08. 10)
   "Explosive Sensing by Two Different Sizes of Luminescent Porous Silicon Particles"